Chaos near the gap soliton in a Kerr grating

Theo P. Valkering* and Arie Irman

*Computational Materials Science, Faculty of Science and Technology and MESA$^+$Research Institute, University of Twente,
P.O. Box 217, 7500 AE Enschede, The Netherlands*
(Received 3 March 2004; published 22 September 2004)

Differences are investigated between solutions of the one-dimensional Helmholtz equation for monochromatic waves in a Kerr grating and its approximation, the (generalized) coupled mode (GCM) equations. First it is pointed out that use of the latter can be justified on the basis of averaging theory, and an upper bound is given for the error made this way. Second, the qualitative difference that arises because of the nonautonomous nature of the Helmholtz equation is investigated. The latter property causes that part of the trajectories to be chaotic, in contrast with the periodicity of the solutions of the (autonomous) GCM equations. In particular, standing waves near the gap soliton with (envelope) wavelength of the order of the inverse squared of the index contrast show irregular features. This is concluded from the observed scaling behavior of the dimensions of the chaotic region in the phase plane.

I. INTRODUCTION

Monochromatic waves with frequency near a band gap in a one-dimensional Kerr grating with period d are usually described by writing the electric field as a sum of two counter-propagating traveling waves with slowly varying amplitudes $A_+(z)$ and $A_-(z)$, say. Approximate equations for these amplitudes are heuristically found on the basis of the *a priori* assumption that the amplitudes depend slowly on z after substitution of the electric field into Maxwell's equations. In this way one obtains the so-called coupled mode equations, cf. Refs. [1,2] and references therein. In a more sophisticated and precise procedure one writes the field as a linear combination of, e.g., Bloch modes, and first sets up exact equations for the amplitudes [3,4]. Subsequently one derives without *a priori* assumptions an approximate version of the equations. This leads, cf. also Ref. [5], to so-called generalized coupled mode (GCM) equations. The latter equations have all the same form but differ in the precise definition of the parameters and the amplitude fields. Investigation of the difference between solutions of the exact equations and of their approximate version is the subject of this paper.

As a first topic it is demonstrated that the GCM equations are obtained from the exact equations by an averaging procedure [6,7]. This procedure yields an overall upper bound for the difference in terms of the (small) parameters: detuning, linear index contrast, and nonlinearity.

Second the qualitative difference between solutions of exact and approximate equations is investigated for a specific case: standing waves in a multilayer. A crucial qualitative difference is expected for the following reason: the exact equations depend periodically on z. Consequently, part of their solutions show irregular, "chaotic" behavior [8,9]. In contrast, the GCM equations, being the averaged version of the exact equations, do not depend explicitly on z. Their Hamiltonian stucture makes them integrable and solutions

are in general doubly periodic, with equilibria and the solutions of infinite period, the gap solitons, as extremal cases (in fact, they are known explicitly, cf. Ref. [2]). This qualitative difference is investigated for standing waves, in particular for those near the gap soliton.

These issues are discussed in the following way. Starting from the Helmholtz equation an equivalent system of two coupled first order equations for the mode amplitudes A_+ and A_- of harmonic modes $\exp(\pm ik_B z)$, $k_B = \pi/d$ is formulated. This provides an exact description of the waves, within the range of validity of the Helmholtz equation. The averaged version of these equations yields the GCM equations and thus error estimates can be obtained in terms of the relevant small parameters.

Next, standing waves in a multilayer are considered in more detail. Via phase plane analysis solutions of the exact equations for the multilayer are compared with those of the corresponding GCM equations. As expected, the former show chaotic behavior. In particular one observes a region with chaotic trajectories around the gap soliton, as the theory of nonintegrable systems predicts. Numerically a scaling result for the dimension of this region is found in terms of the (linear) index contrast of the multilayer. Comparison with the corresponding GCM phase portrait shows that this region contains waves with (envelope) wavelength longer than the inverse squared of the index contrast. Furthermore, the present calculations demonstrate that the GCM model gives a very poor description for index contrast larger than the order of 10^{-1}.

II. EQUATIONS

A. Coupled mode equations and averaging

Consider monochromatic waves in a one-dimensional system with third order nonlinearity. The electric field is orthogonal to the direction of propagation z and given by $\mathrm{Re}[E(z)\exp(i\omega t)]$. The nonlinear index of refraction depends periodically on z with period d and reads, with $\zeta = z/d$,

_____

*Email address: t.p.valkering@utwente.nl

$n(\zeta) = n_0(\zeta) + n_2(\zeta)|E|^2$. Then Helmholtz equation reads

$$d^2\tilde{E}/d\zeta^2 = -d^2 k_0^2(\zeta)[1 + \gamma(\zeta)|\tilde{E}|^2]\tilde{E}, \tag{1}$$

where the different symbols are given by (E_0 is some real reference field)

$$k_0(\zeta) = \frac{\omega}{c} n_0(\zeta), \quad \gamma(\zeta) = \frac{2n_2(\zeta)}{n_0(\zeta)} E_0^2, \quad \tilde{E} = \frac{E}{E_0}. \tag{2}$$

In shallow gratings band gaps occur at frequencies and wave numbers near multiples of the Bragg wave number and frequency $k_B = \pi/d$, $\omega_B = c k_B / \bar{n}_0$, $\bar{n}_0$ denoting the average of $n_0(\zeta)$. To formulate a set of first order equations that is appropriate to describe solutions with frequencies near and in the first band gap, the electric field is written as a linear combination of solutions $\exp(\pm i\pi\zeta)$ of the homogeneous linear part of Eq. (1),

$$\tilde{E}(\zeta) = \frac{1}{\sqrt{2dk_0(\zeta)}}[e^{-i\pi\zeta} A_+(\zeta) + e^{i\pi\zeta} A_-(\zeta)], \tag{3}$$

i.e., as a sum of modulated traveling waves, with A_+ and A_- as amplitudes. The standard way of deriving the CM equations is to assume that these amplitudes depend slowly on ζ, and neglecting small terms. Here we use a different route, similar to the one in Refs. [3,4], leading to GCM. Relation (3) is supplemented with a second relation,

$$\frac{d\tilde{E}}{d\zeta} = i\sqrt{\frac{dk_0(\zeta)}{2}}[-e^{-i\pi\zeta} A_+(\zeta) + e^{i\pi\zeta} A_-(\zeta)], \tag{4}$$

and we consider Eqs. (3) and (4) as a transformation from variables $[\tilde{E}(\zeta), d\tilde{E}/d\zeta]$ to $[A_+, A_-]$. This results in a set of first order equations for A_+ and A_- that is equivalent to Eq. (1). Somewhat lengthy but straightforward calculations show that this set has the form

$$dA_+/d\zeta = -iF(A_+, A_-; \varepsilon, \delta, \mu),$$

$$dA_-/d\zeta = iF(A_-, A_+; \varepsilon^*, \delta, \mu^*) \tag{5}$$

with F given by

$$F = \delta(\zeta)A_+ + \varepsilon(\zeta)A_- + \mu_0(\zeta)\{|A_+|^2 + 2|A_-|^2\}A_+ + \mu_1(\zeta)\{2|A_+|^2 + |A_-|^2\}A_- + \mu_1^*(\zeta)A_+^2 A_-^* + \mu_2(\zeta)A_-^2 A_+^*. \tag{6}$$

F depends periodically on ζ through the ζ-dependent "parameter functions" $\varepsilon(\zeta)$, $\delta(\zeta)$, and $\mu_n(\zeta)$,

$$\delta(\zeta) = dk_0(\zeta) - \pi, \quad \varepsilon(\zeta) = \frac{in_0'(\zeta)}{2n_0(\zeta)} e^{2i\pi\zeta},$$

$$\mu_n(\zeta) = \frac{\gamma(\zeta)}{4} e^{in2\pi\zeta}. \tag{7}$$

The generalized coupled mode equations are Eqs. (5) and (6) with the parameter functions (7) replaced by their averaged values. One way to justify this replacement is to assume that the averaged values $\bar{\delta}$, $\bar{\varepsilon}$, $\bar{\mu}_n$ are small and that the coefficients satisfy the order relations $\delta(\zeta) = O(\bar{\delta})$, etc. Then,

applying the averaging method [6,7], one concludes that *the difference between the solutions of the full and the averaged equations for initial condition that differ in first order in the small parameters, remains of first order on a distance scale of order of their inverse.* In Appendix A 1 a more precise formulation of how to obtain this result is given.

In applications, the parameter functions in Eq. (7) depend on a fewer number of small parameters, for instance the detuning $(\omega - \omega_B)/\omega_B$, the linear index contrast ε introduced through

$$n_0(\zeta) = \bar{n}_0[1 + \varepsilon\, s(\zeta)], \tag{8}$$

and the nonlinearity μ via $n_2(\zeta) = \mu\, m(\zeta)$. Here $s(\zeta)$ and $m(\zeta)$ are arbitrary but fixed functions, determined by the gratings one wants to consider. If $s(\zeta)$ has zero average one readily evaluates that the averaged values satisfy

$$\bar{\delta} = \delta(\omega - \omega_B)/\omega_B,$$

$$\bar{\varepsilon} = \varepsilon\left[\frac{i}{2}\left(\frac{d}{d\zeta}\ln n_0(\zeta)\right)e^{2i\pi\zeta}\right]_{av} + O(\varepsilon^2),$$

$$\bar{\mu}_n = \mu\frac{E_0^2}{2\bar{n}_0}[m(\zeta)e^{in2\pi\zeta}]_{av} + O(\varepsilon\mu). \tag{9}$$

Thus the averages are of first order in δ, ε, and μ. The same holds for the functions themselves. Consequently in the averaged equations one may retain only the terms that are linear in δ, ε, and μ.

B. Equations for a multilayer

Here we consider a multilayer where each unit consists of two layers, a and b with indices of refraction denoted by $n_{0a,b}$ and $n_{2,ab}$, respectively. Then the parameter functions $\delta(\zeta)$, $\mu_n(\zeta)$ in Eq. (7) and $s(\zeta)$ in Eq. (8) are step functions, and $\varepsilon(\zeta)$ equals the sum of two δ functions located at the transition points between the layers. These properties cause that averaging theory as it is formulated usually cannot be applied immediately.

Maintaining the aim of the present paper, F in Eq. (6) was simplified by taking $\mu_1 = \mu_2 = 0$. Having in mind that $\varepsilon(\zeta) = 0$ within each homogeneous layer, one sees that coupling between A_+ and A_- is then realized by the nonlinear self- and cross-phase modulation within each layer, and by the linear coupling at the transition between the layers. This simplification allows us to give an explicit expression for the transfer map for the full system. In Appendix A 2 it is shown that the averaged system as defined above is the proper one for this transfer map.

The full equations are periodic in ζ, and a standard way to investigate their solutions is via the transfer map $\mathcal{T}$ over one unit. For the present problem this map can be given explicitly. Let A denote the column vector $[A_+, A_-]^T$. Then essential features of the trajectories are represented by the discrete sequence, generated by $\mathcal{T}$,
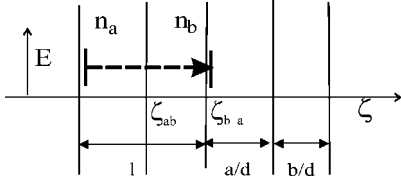
FIG. 1. Definition of grating geometry.

$$A_n = \mathcal{T}(A_{n-1}), \quad \{A_n = A(\zeta_o + n)\}, \tag{10}$$

where ζ_0 is an arbitrarily chosen initial position. Let ζ_0 be at the beginning of a layer a. Then $\mathcal{T}$ is given by the composed transformation (cf. Fig. 1)

$$\mathcal{T} = B_{ba} \circ \Phi_b \circ B_{ab} \circ \Phi_a. \tag{11}$$

Here $\Phi_{a,b}$ is the flow through the layers a and b, respectively, and the matrices $B_{ab,ba}$ represent the transition between the two materials, from a to b (b to a). Here note that $n_0(\zeta)$ is discontinuous at a boundary between two layers, so that the transformation Eq. (3) and (4) is discontinuous as well. Therefore the variables A are discontinuous at the transition point, and there is a linear relation between the values at each side of the boundary. One writes $A_b = B_{ab}A_a$ at the boundary from a to b. This transformation is found from the continuity of E and $dE/d\zeta$. With Eqs. (3) and (4) one finds straightforwardly

$$B_{ab} = \begin{bmatrix} \beta_+ & \beta_- e^{2i\pi\zeta_{ab}} \\ \beta_- e^{-2i\pi\zeta_{ab}} & \beta_+ \end{bmatrix}, \tag{12}$$

with

$$\beta_\pm = \frac{1}{2}(\rho \pm \rho^{-1}), \quad \rho = \sqrt{\frac{n_{0b}}{n_{0a}}} \tag{13}$$

and ζ_{ab} denoting the position of the boundary.

In the nonlinear material, an explicit expression for the flow $\Phi_{a,b}$ follows from Eqs. (5) and (6) with $\varepsilon(\zeta) = 0$ and $\mu_1(\zeta) = \mu_2(\zeta) = 0$. With the definitions

$$\kappa_{a,b\pm}(A_+, A_-) = \delta_{a,b} + \mu_{0a,b}\{|A_\pm|^2 + 2|A_\mp|^2\}, \tag{14}$$

Φ_a can be written in the form of a matrix, depending nonlinearly on its argument,

$$\Phi_a(A) = \begin{bmatrix} e^{-i\kappa_a(A_+, A_-)(a/d)} & 0 \\ 0 & e^{i\kappa_a(A_+, A_-)(a/d)} \end{bmatrix} \begin{bmatrix} A_+ \\ A_- \end{bmatrix} \tag{15}$$

and similar for Φ_b.

To obtain the averaged equations observe that $\varepsilon(\zeta)$ contains two δ functions at the material boundaries ζ_{ab} and ζ_{ba}. Thus $\bar{\varepsilon}$ consists of contributions of two terms. Evaluating the first contribution yields after partial integration

$$\lim_{\lambda \to 0} \int_{\zeta_{ab}-\lambda}^{\zeta_{ab}+\lambda} \varepsilon(\zeta)d\zeta = \frac{i}{2}e^{2i\pi\zeta_{ab}} \ln\frac{n_b}{n_a} \tag{16}$$

and similar for the second. Then, with $\zeta_{ab} = \zeta_{ba} + a/d$ one finds
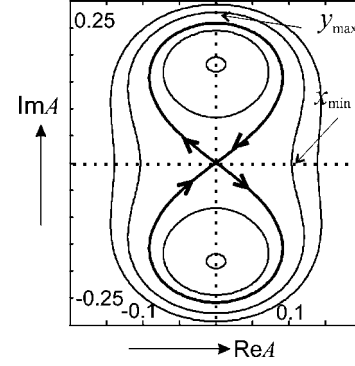
FIG. 2. Level sets of the Hamiltonian at mid gap frequency $\bar{\delta} = 0$, $\bar{\mu} = 1$, $\bar{\varepsilon} = 0.1$. Thick: the gap soliton.

$$\bar{\varepsilon} = \ln\frac{n_a}{n_b}e^{i\pi(2\zeta_{ba}+a/d)} \sin(\pi a/d). \tag{17}$$

Clearly $\bar{\varepsilon}$ is complex, but always can be chosen to be real by proper choice of the origin of the ζ axis. Because of the underlying Hamiltonian structure, the equation has a constant of the motion, the Hamiltonian **H**, which is given by ($\bar{\varepsilon}$ is chosen to be real and $\bar{\mu}$ stands for $\bar{\mu}_0$ which is real)

$$\mathbf{H} = \bar{\delta}(|A_+|^2 + |A_-|^2) + \bar{\varepsilon}(A_-^*A_+ + A_-A_+^*) + \frac{\bar{\mu}}{2}[|A_+|^4 + |A_-|^4$$
$$+ 4|A_+|^2|A_-|^2]. \tag{18}$$

Trajectories are most easily represented in terms of the level sets of this Hamiltonian.

III. STANDING WAVES NEAR THE GAP SOLITON IN THE MULTILAYER

In this section the trajectories of standing wave solutions of Eq. (5) with $\mu_1(\zeta) = \mu_2(\zeta) = 0$ are compared with those of its averaged counterpart at $\bar{\delta} = 0$, i.e., ω is at the Bragg frequency $c\,\bar{n}_0^{-1}k_B$. Standing waves can be chosen to have real $E(z)$. Consequently $A_+ = A_-^* = A = |A|\exp(i\phi_A)$, say, and trajectories are drawn in the complex A plane. The electric field then can be written as, cf. Eq. (3),

$$E(z) = \sqrt{\frac{2}{dk_0(z/d)}}|A(z/d)|\cos[\pi z/d + \phi_A(z/d)]. \tag{19}$$

A. Periodic solutions of the averaged equations

Trajectories of the averaged system are most easily represented as level curves (Fig. 2) of the averaged Hamiltonian (18) which with $A = (x+iy)/2$ reads

$$\mathbf{H} = \frac{1}{2}\bar{\delta}(x^2 + y^2) + \frac{1}{2}\bar{\varepsilon}(x^2 - y^2) + \frac{3}{16}\bar{\mu}(x^2 + y^2)^2. \tag{20}$$

The (two) trajectories through the origin, so-called homoclinic loops, represent a localized excitation, the gap soliton. The smooth closed curves both inside and outside the homoclinic loops represent periodic trajectories $A(\zeta)$ with

period depending on the value of H, with a singularity at $H=0$. For the gap soliton the maximum value of the electric field occurs where level sets intersect the imaginary axis, i.e., where $\mathbf{H}(0,y)=0$. One finds with Eqs. (20) and (3)

$$\bar{\mu}|A_{\max\;sol}|^2 = \frac{2}{3}\bar{\varepsilon}, \quad \bar{n}_2|E_{\max\;sol}|^2 = \frac{4}{3}\bar{n}_0\bar{\varepsilon}. \quad (21)$$

The amplitude of the periodic solutions varies between values $|A_{\min}|$ and $|A_{\max}|$, determined by the intersection of the closed curves with the imaginary axis, for inside and outside trajectories given by

$$\mathbf{H}(0,y_{\max}) = \mathbf{H}(0,y_{\min}) = H \quad \text{if} \quad H < 0,$$

$$\mathbf{H}(0,y_{\max}) = \mathbf{H}(x_{\min},0) = H \quad \text{if} \quad H > 0. \quad (22)$$

In either case $y_{\max}$ approaches the value in Eq. (21) when $H \rightarrow 0$ and $x_{\min}$ and $y_{\min}$ tend to zero.

For trajectories near the gap soliton, the wavelength can be expressed approximately in terms of these maximum and minimum values as follows. If $\tilde{P}(H)$ denotes the distance that is covered by a trajectory in the first quadrant, then the wavelength of the inner and outer trajectory is given by $P_{in}=2\tilde{P}$ and $P_{out}=4\tilde{P}$, respectively. In Appendix B it is shown that

$$\bar{\varepsilon}\tilde{P} = \ln\frac{|A_{\max}|}{|A_{\min}|} + \text{terms bounded when } H \rightarrow 0. \quad (23)$$

Clearly the first term diverges when $H \rightarrow 0$, so it is the dominant one. This term is easily understood as follows: Near the origin a trajectory is approximately a linear combination of the two eigenmodes $\exp(\pm\zeta\sqrt{\bar{\varepsilon}^2-\bar{\delta}^2})$ of the linearized system. Consequently when $\bar{\delta}=0$, the amplitude grows as $|A| \sim |A_{\min}|\exp(\bar{\varepsilon}\zeta)$. Now observe that for small $|A_{\min}|$ and small $\bar{\varepsilon}$ the trajectory remains extremely long in the neighborhood of the origin, so that the period is dominated by the linear growth from $|A_{\min}|$ to $|A_{\max}|$. The actual proof of Eq. (23) is based on this argument (cf. Appendix B). Note that this expression makes sense only if $|A_{\min}| \ll |A_{\max}|$ and small $\bar{\varepsilon}$.

B. Irregular solutions of the full equations

With the transfer map (11), a series of phase portraits, cf. Fig. 3, was calculated for different values of the index contrast defined as $\varepsilon=(n_{0a}-n_{0b})/(n_{0a}+n_{0b})$. The phase portraits show, apart from a scaling factor, discrete trajectories of $\tilde{A} = \exp(-i\pi\zeta)A$, the right going constituent of the electric field in Eq. (3). Note that $\tilde{A}_n=(-)^n A_n$. They are obtained using the transfer map using the code accompanying Ref. [12]. For comparison of averaged results with the exact ones note that $\bar{\varepsilon}=\ln(n_a/n_b)=2\varepsilon+O(\varepsilon^2)$.

One directly sees that for the smaller values of ε the phase portrait is similar to that of the averaged model, apart from a rotation due to the choice of ζ_0 in Eq. (10). With increasing ε one sees a growing dark region around the homoclinic loop that exists for $\varepsilon=0$. The equilibria inside the (former) homoclinic loops remain, with closed curves around them. Outside the loops one observes closed curves as well, they dis-

appear, however, completely for the larger values of ε.

Here we focus on the dense collection of dots in the neighborhood of the unstable manifold. These dots determine a region whose dimensions grow with increasing ε. We will call this region $\mathcal{C}$. In each graph in Fig. 3, this region is generated by one initial condition only, nearby the origin. Any starting point within $\mathcal{C}$ fills this region.

To investigate the way in which the dimensions of $\mathcal{C}$ depend on ε, both D and the diameter R of the largest circle around the origin that fits within $\mathcal{C}$ were determined as functions of ε, cf. Figs. 4 and 5. A fit yields the following scaling relations:

$$D = c_1 \varepsilon^{1/2} \quad \text{and} \quad R = c_2 e^{-c_3/\varepsilon} \quad (24)$$

with constants approximately $c_1=5$, $c_2=232$, $c_3=1$. One observes that D^2 is approximately linear in ε, which agrees with the relationship (21) that follows from the averaged equations. R becomes small with $\exp(-c_3/\varepsilon)$.

The values of the constants c_i depend on the specific system one is considering, but the functional dependence of ε is expected to be universal for the type of problem considered here. It seems remarkable that c_3 approximately equals unity. However, in terms of scaling this cannot be relevant, since a change of the definition of ε changes the value of this constant. This exponential behavior is not unexpected. For a perturbed Hamiltonian oscillator the perturbation leads to exponential splitting of the homoclinic trajectory [10], which splitting determines the dimensions of the stochastic layer $\mathcal{C}$. Related to this the dynamics near the separatrix and the width of the layer can be approximately described by the so-called whisker map, cf. Ref. [8] (for an example yielding exponential width, cf. Ref. [11]).

C. Interpretation

The phase portraits in Fig. 3 are typical for a two-dimensional (2D) dynamical system that can be seen as a perturbed integrable system, as the present one. For a proper interpretation one needs the concepts and theories that describe the changes with respect to the averaged integrable model: *KAM theory* (the survival or disappearance of periodic orbits whose period is irrational with respect to the lattice period d), *Poincare-Birkhoff theory* (the survival of rational periodic orbits), and *Chaos theory*, the appearance of irregular trajectories, cf. Refs. [8,9,12]. Typical trajectories in a chaotic region show sensitivity of initial conditions, i.e., two trajectories that start nearby each other grow exponentially apart with distance. Furthermore, the Fourier spectrum of a trajectory is broadened compared to the δ function spectrum of the periodic orbits in the unperturbed averaged system.

Comparing the phase portraits in Fig. 3 with those of the averaged system, Fig. 2, one infers that a set of periodic trajectories around the gap soliton and with a certain range of frequencies have lost their periodicity. To quantify this statement, observe that the phase portraits in Fig. 3 suggest that there is a largest inner closed curve and a smallest outer curve roughly at the boundary of $\mathcal{C}$. Using the approximate
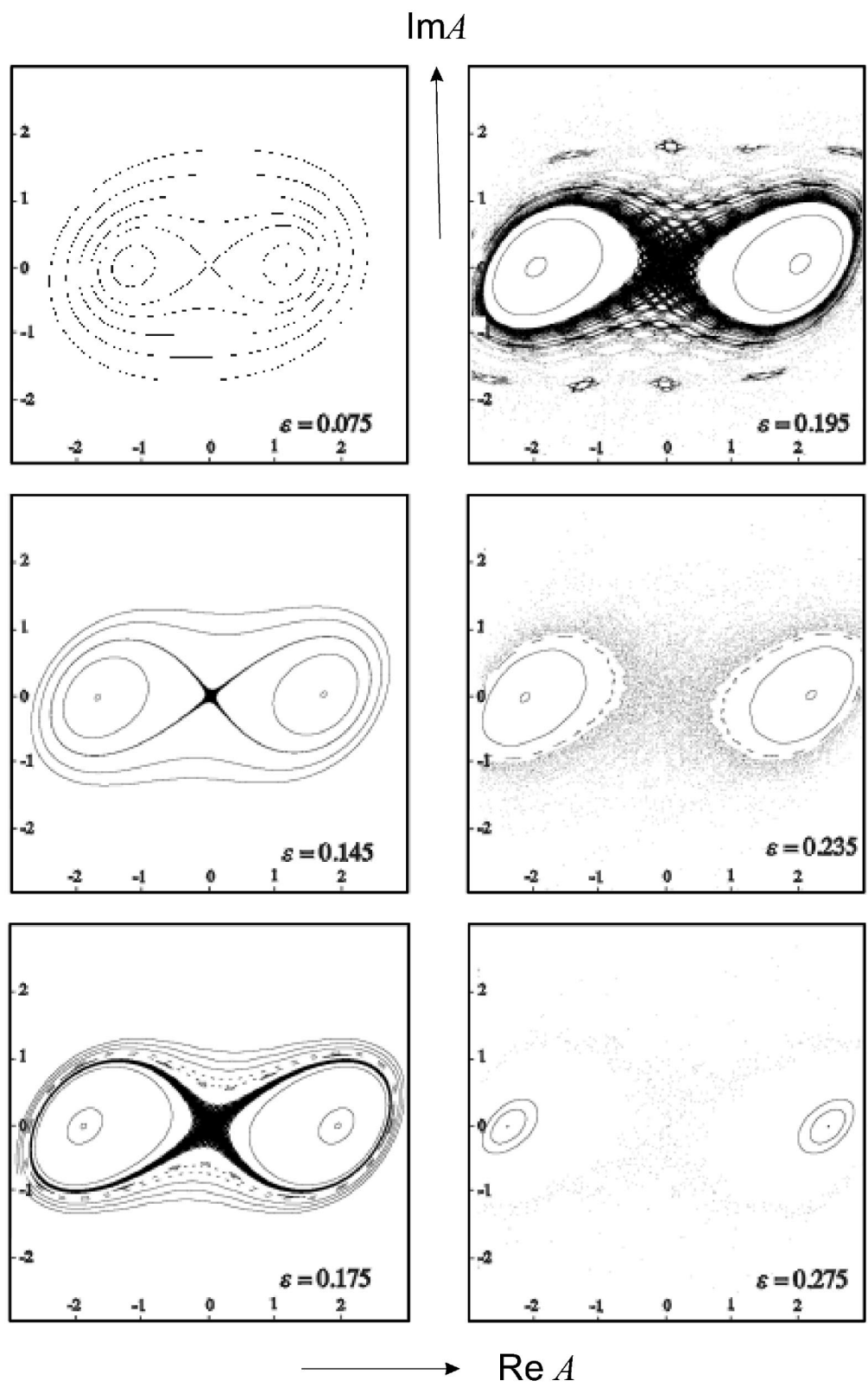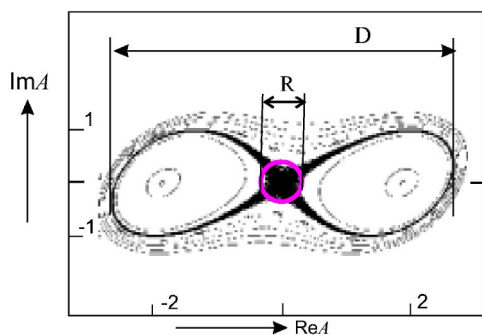
FIG. 3. Discrete phase portraits of the transfer map for increasing linear index contrast $\varepsilon=(n_{0a}-n_{0b})/(n_{0a}+n_{0b})$ (top to bottom). They demonstrate the growth of the chaotic region near the homoclinic loop (the gap soliton); $n_0=2$, $n_{2a}=0$, and the reference field $E_0^2 =2(3n_{2b}n_b)^{-1}$.

FIG. 4. Definitions of D and R.

expression for the period (23), one infers from the scaling results (24) that the period of the outer surviving curve is determined by

$$P_{out} \sim \bar{\varepsilon}^{-1} \ln(D^2/R^2) = \bar{\varepsilon}^{-1}\{\ln c_5 + \ln\bar{\varepsilon} + 2c_3\bar{\varepsilon}^{-1}\}. \quad (25)$$

The dominant term is of order $\bar{\varepsilon}^{-2}$. For the period of the inner orbit, one obtains a similar expression. We conclude that the periodic orbits in the averaged model with period larger than the order of magnitude of $\bar{\varepsilon}^{-2}$ haved turned into irregular trajectories.

The irregularity of a typical trajectory appears as follows: In the averaged model, the trajectories inside a homoclinic loop circle around one of the equilibria. Correspondingly the phase of A oscillates around $\pi/2$ ($-\pi/2$). The trajectories outside the loops circle alternatingly around the two equilibria, i.e., the phase jumps with π each period of the amplitude $|A|$. In either case a trajectory forms a sequence of localized excitations at a regular distance. In contrast a typical trajectory in region $\mathcal{C}$ will swap at irregular intervals between the two regions. More specifically, for any given initial condition there exists a sequence of numbers $\{N_1,N_2,N_3,\ldots\}$ with random properties where N_n denotes the number of times the trajectory encircles one equilibrium. This fact leads to irregular behavior of the phase of the electric field, cf. Eq. (19), in
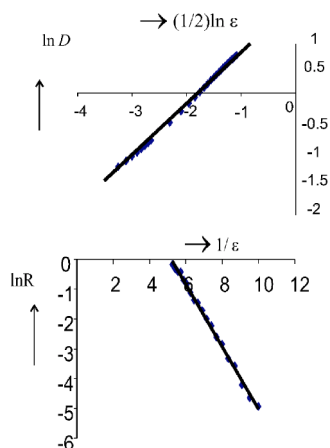
FIG. 5. Scaling results for D and R as function of index contrast.

sharp contrast to the phase behavior of the field in the averaged model. This behavior depends sensitively on the initial condition. That means that two trajectories that are very close at $\zeta=\zeta_0$ typically will finally have completely different sequence $\{N_1,N_2,N_3,\ldots\}$.

IV. DISCUSSION

Summarizing, it was pointed out that solutions of the generalized coupled mode equations and the corresponding solutions of the Helmholtz equation grow apart at no more than the order of the small parameters (i.e., detuning, linear index contrast $\bar{\varepsilon}$, and nonlinearity) on a distance proportional to their inverse. In particular, restricting this result to the linear index contrast, it says that trajectories in full and averaged model, respectively, that are $\bar{\varepsilon}$ close at $\zeta=0$, remain $\bar{\varepsilon}$ close at distance $O(\bar{\varepsilon}^{-1})$. Complementary to this, for the present multilayer and with ω equal to the Bragg frequency, we observe that a qualitative difference appears for trajectories with wavelength larger than the order of $\bar{\varepsilon}^{-2}$, near the gap soliton. This difference appears primarily in irregular behavior of the phase of the envelope of the electric field.

The area in the phase portrait filled by these irregular trajectories, diminishes exponentially as a power of $\exp(-\bar{\varepsilon}^{-1})$. So it becomes extremely small for fiber gratings, with index contrast of the order of 10^{-3}, 10^{-4}. In contrast, for values of $\bar{\varepsilon}$ of order 1, the phase portraits of the Helmholtz equation and GCM disagree completely, as Fig. 3 shows. Note, however, that results are obtained for varying the index contrast with frequency fixed at the Bragg value. Complementary, the scaling behavior should be investigated fixing the index contrast and varying the frequency, in which case one explores the solutions near the edge of the band gap.

Finally, to compare the averaging result with the irregular properties found, recall that chaos theory says that two trajectories in the full equations on the average grow apart at a rate of $\exp(\lambda\zeta)$, where λ is the so-called Lyapunov exponent. In the chaotic region $\mathcal{C}$, λ is expected to be of the order of the eigenvalues of the origin, i.e., $\lambda\sim\bar{\varepsilon}$. Consequently, at a distance of order $O(\bar{\varepsilon}^{-1})$ the growth factor is $\exp(\lambda\zeta)=O(1)$, so that chaotic effects do not appear and, in agreement with the averaging result, trajectories do not grow apart. On the other hand, trajectories of period of order $\gtrsim\bar{\varepsilon}^{-2}$ of the averaged system have erratic phase behavior. Indeed, on such a length scale the growth factor $\exp\lambda\zeta\sim\exp(\bar{\varepsilon}^{-1})$ is much bigger than unity, and the averaged equations cannot be expected to be useful. Thus one sees that the length scales at which chaos is observed here and where the averaged equations are valid do not overlap.

ACKNOWLEDGMENT

APPENDIX A: AVERAGING

1. Applying the averaging method

Consider F as used for the multilayer,

$$F(A_+, A_-, \zeta) = \delta(\zeta)A_+ + \varepsilon(\zeta)A_- + \mu(\zeta)\{|A_+|^2 + 2|A_-|^2\}A_+.$$
(A1)

Let the parameter functions be real continuous and small with their averages, i.e., $\delta(\zeta) = O(\bar{\delta})$, and similar for the other two parameter functions. Instead of three small parameters, one single small parameter α is introduced as

$$\alpha = \sqrt{\bar{\delta}^2 + \bar{\varepsilon}^2 + \bar{\mu}^2}, \quad \hat{\delta} = \frac{\bar{\delta}}{\alpha}, \quad \text{and} \quad \tilde{\delta}(\zeta) = \frac{\delta(\zeta)}{\alpha}. \quad \text{(A2)}$$

The hat parameters satisfy $\hat{\delta}^2 + \hat{\varepsilon}^2 + \hat{\mu}^2 = 1$ and determine a direction in the 3D sphere around zero in parameter space, α being the radius. The "wiggle" parameter functions are order 1. The equation now reads $dA/d\zeta = \alpha f(A; \tilde{\delta}, \tilde{\varepsilon}, \tilde{\mu})$ with $A = [A_+, A_-]^T$, $f = [-iF(A; \tilde{\delta}, \tilde{\varepsilon}, \tilde{\mu}), iF(A; \tilde{\delta}, \tilde{\varepsilon}, \tilde{\mu})]^T$. Having formulated the equation this way, one can apply the averaging theorem as, e.g., in Refs. [6,7]. Following the proof, one sees that the estimates can be made uniform in the hat parameters and conclude that these estimates apply in a sphere in the original parameter space.

This result makes clear that transformations that differ from those in Eqs. (3) and (4) in first order do not improve the approximation within the accuracy given by averaging result (although in practice it may yield a better result). An obvious example is when $k_0(\zeta)$ in Eqs. (3) and (4) is replaced by its averaged value k_B. Then one finds for the coupled mode variables a vector field as in Eq. (6), but with parameter functions that differ from the ones given here. One can verify that the averaged values of these coefficients are equal to those given in Eq. (7), so that the averaged equations are the same. Note, however, that the variables $A_\pm$ differ, however, in first order, so that no inconsistency with the averaging result arises.

2. Averaging for the multilayer

These proofs mentioned above are formulated for parameter functions that is continuous in ζ. In the case of a multilayer, however, there appears a discontinuity, and even a δ function in Eq. (A1). It requires a more detailed analysis to include such cases in general, which is not the purpose of this paper. Instead we will show that the transfer map (10) equals the transfer map of the averaged equation apart from a term of order α^2. This implies that the difference after applying the map α^{-1} times reduces to order α, as in the averaging result. Thus the averaged version of Eq. (A1) is the proper one for the multilayer.

Essential in the argument is that the map at the material boundaries (12) can be expressed in terms of F as follows. The δ function occurs in $\varepsilon(\zeta)$ only. The corresponding term in F reads

$$\frac{n_0'}{2n_0} \begin{bmatrix} 0 & e^{2i\pi\zeta} \\ e^{-2i\pi\zeta} & 0 \end{bmatrix} \begin{bmatrix} A_+ \\ A_- \end{bmatrix}.$$

Since this term is linear a reasonable choice for the jump in A for a transition from a to b at $\zeta = \zeta_{ab}$ is

$$A_b = \exp\left\{ \lim_{\lambda \to 0} \int_{\zeta_{ab}-\lambda}^{\zeta_{ab}+\lambda} \frac{n_0'}{2n_0} K \, d\zeta \right\} A_a, \quad \text{(A3)}$$

where K denotes

$$K(\zeta) = \begin{bmatrix} 0 & e^{2i\pi\zeta} \\ e^{-2i\pi\zeta} & 0 \end{bmatrix}.$$

This expression yields B_{ab} as will be shown now.

The exponent in this expression can be expressed in the earlier defined $\rho = (n_{0b}/n_{0a})^{1/2}$ in Eq. (13),

$$\lim_{\lambda \to 0} \int_{\zeta_{ab}-\lambda}^{\zeta_{ab}+\lambda} \frac{n_0'(\zeta)}{2n_0(\zeta)} K(\zeta) d\zeta = (\ln \rho) K(\zeta_{ab}). \quad \text{(A4)}$$

To evaluate the linear transformation in Eq. (A3) one diagonalizes the exponent

$$K(\zeta_{ab}) = U \begin{bmatrix} 1 & 0 \\ 0 & -1 \end{bmatrix} U^{-1},$$

where

$$U = \frac{1}{\sqrt{2}} \begin{bmatrix} e^{i\pi\zeta_{ab}} & e^{i\pi\zeta_{ab}} \\ e^{-i\pi\zeta_{ab}} & -e^{-i\pi\zeta_{ab}} \end{bmatrix}. \quad \text{(A5)}$$

Then using the general equality $\exp(UMU^{-1}) = U(\exp M)U^{-1}$ one finds straightforwardly that $\exp\{\ln \rho \, K(\zeta_{ab})\}$ equals

$$\frac{1}{2} \begin{bmatrix} \rho + \rho^{-1} & (\rho - \rho^{-1})e^{2i\pi\zeta_{ab}} \\ (\rho - \rho^{-1})e^{-2i\pi\zeta_{ab}} & (\rho + \rho) \end{bmatrix}, \quad \text{(A6)}$$

which expression equals B_{ab} in Eq. (12).

Comparison of the averaged and the exact transfer maps

An approximate expression for the map of the averaged equation $dA/d\zeta = \alpha f_{av}(A; \hat{\delta}, \hat{\varepsilon}, \hat{\mu})$ is obtained as follows. This map satisfies $A(1) = A(0) + \alpha \int_0^1 f_{av}[A(\zeta)] \, d\zeta$ and since $A(\zeta) = A(0) + O(\alpha)$ for $0 < \zeta < 1$ it holds

$$A(1) = \{Id + \alpha f_{av}(\cdot) + O(\alpha^2)\}A(0) \quad \text{(A7)}$$

with $f_{av}(\cdot)$ denoting the nonlinear transformation $f_{av}(\cdot)A = f_{av}(A)$.

Next consider the transfer map $\mathcal{T}$ in Eq. (10). Observe for $\alpha = 0$ its constituents are all equal to Id, and we consider the first order correction. Within one layer the coefficients in F are constants and it holds

$$\Phi_a(\cdot) = Id + \alpha \, af_a(\cdot) + O(\alpha^2). \quad \text{(A8)}$$

Here the subscript a denotes the value of the field in medium a. Recall that $\alpha f_a(A) = [-iF_a(A_+, A_-), iF_a(A_-, A_+)]^t$. With the result in Eqs. (A3) and (A6) one obtains similarly

$$B_{ab} = Id + \alpha \lim_{\lambda \to 0} \int_{\zeta_{ab}-\lambda}^{\zeta_{ab}+\lambda} f_\varepsilon + O(\alpha^2), \quad \text{(A9)}$$

where f_ε denotes the linear term in f that corresponds to

$\varepsilon(\zeta)$. A similar relation holds for B_{ba}. Now consider the composed mapping $\mathcal{T}$ to find

$$\mathcal{T} = Id + \alpha \left\{ \begin{array}{l} \dfrac{a}{d} f_a(\cdot) + \displaystyle\lim_{\lambda \to 0} \int_{-\lambda + \zeta_{ab}}^{+\lambda + \zeta_{ab}} f_\varepsilon + \\[4mm] + \dfrac{b}{d} f_b(\cdot) + \displaystyle\lim_{\lambda \to 0} \int_{-\lambda + \zeta_{ba}}^{+\lambda + \zeta_{ba}} f_\varepsilon \end{array} \right\} + O(\alpha^2). \tag{A10}$$

Since

$$\lim_{\lambda \to 0} \int_{-\lambda + \zeta_{ab}}^{+\lambda + \zeta_{ab}} f_\varepsilon = \lim_{\lambda \to 0} \int_{-\lambda + \zeta_{ab}}^{+\lambda + \zeta_{ab}} f(\cdot) \tag{A11}$$

and f_a and f_b do not depend on ζ we can combine the four terms to

$$\mathcal{T} = Id + \alpha \, f_{av}(\cdot) + O(\alpha^2) \tag{A12}$$

so that comparing with Eq. (A7) we obtain the required result.

APPENDIX B: SINGULARITY IN THE WAVELENGTH

Smooth closed curves in the phase portrait in Fig. 2 represent waves with periodic trajectories with period P that depends on H, as sketched. Here we derive an approximate expression for P as function of H near $H=0$. We consider a trajectory just outside the homoclinic loop, and correspondingly the behavior for $H \downarrow 0$. The proof for the inner trajectories runs similarly.

An exact expression as a function of the value of H follows from the Hamiltonian form of the equations $dx/d\zeta = \partial \mathbf{H}/\partial y$, $dy/d\zeta = -\partial \mathbf{H}/\partial x$ with $\mathbf{H}$ as in Eq. (20) and is given by $P(H) = \oint ds/\|\nabla \mathbf{H}\|$, where the integral is taken over the closed loop corresponding to $\mathbf{H} = H$. To find an approximate expression for P when H is near zero, we proceed as follows. For the present Hamiltonian the trajectory just outside the homoclinic loop is described by a function $\bar{x}(y; H)$, such that $\mathbf{H}(\bar{x}, y) = H$. This function is defined on the interval $[0, y_m]$ and connects in the x-y plane the points $\{x_m, 0\}$ and $\{0, y_m\}$. Here x_m and y_m are the positive solutions of $H = \mathbf{H}(x_m, 0)$ and $H = \mathbf{H}(0, y_m)$, respectively [x_{min} and y_{max} in the text, cf. Eq. (22)]. This function describes $1/4$ of a complete closed trajectory. Then with $\mathbf{H}(\bar{x}, y) = H$ one finds that $(\partial \mathbf{H}/\partial x) \times (d\bar{x}/dy) + \partial \mathbf{H}/\partial y = 0$, and one transforms the exact expression for $P(H)$ given above to

$$P = 4\tilde{P}, \tilde{P} = \left| \int_0^{y_m} (\partial \mathbf{H}/\partial x)^{-1} \, dy \right|. \tag{B1}$$

Here it will be shown for $\bar{\delta} = 0$ that $\tilde{P}$ can be written as

$$\bar{\varepsilon} \tilde{P} = \ln(y_m/x_m) + \text{terms bounded in } H \text{ when } H \downarrow 0. \tag{B2}$$

To obtain this result, observe that both y_m and the integrand, through $\bar{x}(y; H)$, depend on H. For $H \to 0$ the value of $y_m(H)$ converges to the solution of $\mathbf{H}(0, y_M) = 0$ given by

$$3\bar{\mu} y_M^2 = 8(\bar{\varepsilon} - \bar{\delta}). \tag{B3}$$

To simplify the integral we introduce scaled variables and Hamiltonian

$$\xi = \frac{x}{y_M}, \quad \eta = \frac{y}{y_M}, \quad \tilde{\mathbf{H}}(\xi, \eta) = \frac{16}{3\bar{\mu} y_M^4} H(y_M \xi, y_M \eta) \tag{B4}$$

and evaluate $\tilde{\mathbf{H}}$ to find

$$\tilde{\mathbf{H}}(\xi, \eta) = \xi^2 \frac{\bar{\varepsilon} + \bar{\delta}}{\bar{\varepsilon} - \bar{\delta}} - \eta^2 + (\xi^2 + \eta^2)^2. \tag{B5}$$

Then with $\partial \tilde{\mathbf{H}}/\partial \xi = [(3/16)]\bar{\mu} y_M^4)^{-1}(\partial \mathbf{H}/\partial x) y_M$ one writes Eq. (B1) as

$$\tilde{P} = \frac{2}{\bar{\varepsilon} - \bar{\delta}} \left| \int_0^{y_m/y_M} (\partial \tilde{\mathbf{H}}/\partial \xi)^{-1} \, d\eta \right|, \tag{B6}$$

where use is made of Eq. (B3).

Analysis

The integral in Eq. (B6) diverges for $\tilde{H} \downarrow 0$. Expecting that the linearized part of the equations is responsible for this singularity we write $\tilde{P} = \tilde{P}_{lin} + \tilde{P}_{rest}$, which terms, in case that $\bar{\delta} = 0$, are defined as, cf. Eq. (B5),

$$\bar{\varepsilon} \tilde{P}_{lin} = 2 \int_0^{y_m/y_M} \frac{1}{2\sqrt{\eta^2 + \tilde{H}}} d\eta \tag{B7}$$

and

$$\bar{\varepsilon} \tilde{P}_{rest} = 2 \int_0^{y_m/y_M} R(\eta, \tilde{H}) d\eta, \tag{B8}$$

where R given by $R = (\partial \tilde{\mathbf{H}}/\partial \xi)^{-1} - (2\sqrt{\eta^2 + \tilde{H}})^{-1}$. Evaluation of $\tilde{P}_{lin}$ yields

$$\bar{\varepsilon}\tilde{P}_{lin} = \ln(\tilde{H}^{-1/2}) + \ln\left[\frac{y_m}{y_M} + \sqrt{\left(\frac{y_m}{y_M}\right)^2 + \tilde{H}}\right]. \quad (B9)$$

Clearly, the second term is bounded when $\tilde{H} \to 0$. Then, for the first term, it remains to express $\tilde{H}^{-1/2}$ in the ratio ξ_m/η_m. Solving $\tilde{H} = \tilde{\mathbf{H}}(\xi_m, 0)$ one finds $\xi_m^2 = \tilde{H} + O(\tilde{H}^2)$ and similarly $\eta_m^2 = 1 + \tilde{H} + O(\tilde{H})^2$ so that

$$x_m/y_m = \tilde{H}^{1/2}[1 + O(\tilde{H})] \quad (B10)$$

showing that Eq. (B2) holds for $\bar{\varepsilon}\tilde{P}_{lin}$.

To evaluate $\tilde{P}_{rest}$ evaluate R at $\tilde{H} = 0$. One finds, where $\bar{\bar{\xi}}_0$ stands for $\bar{\xi}(\eta, 0)$,

$$2R(\eta, 0) = \frac{\eta - \bar{\bar{\xi}}_0 - 2\bar{\bar{\xi}}_0^3 - 2\bar{\bar{\xi}}_0 \eta^2}{\eta \bar{\bar{\xi}}_0[1 + 2\bar{\bar{\xi}}_0^2 + 2\eta^2]}. \quad (B11)$$

Since $\xi = \bar{\xi}(\eta, 0)$ satisfies $\bar{\xi}(\eta, 0) = \eta[1 + O(\eta^2)]$ one sees that $R(\eta, 0) = \eta + h.o.t.$ As a result $\tilde{P}_{rest}(\tilde{H} = 0)$ is bounded, and since $\tilde{P}_{rest}$ depends continuously on $\tilde{H}$ one concludes that Eq. (B2) holds for $\tilde{P}_{rest}$ as well.

---

[1] H. G. Winful, J. H. Marburger, and E. Garmire, Appl. Phys. Lett. **35**, 379 (1979).

[2] C. M. de Sterke and J. E. Sipe, in *Progress in Optics Vol. XXXIII*, edited by E. Wolf (Elsevier, New York, 1994).

[3] D. G. Salinas, C. M. de Sterke, and J. E. Sipe, Opt. Commun. **111**, 105 (1994).

[4] C. M. de Sterke, D. G. Salinas, and J. E. Sipe, Phys. Rev. E **54**, 1969 (1996).

[5] T. Iizuka and C. Martijn de Sterke, Phys. Rev. E **61**, 4491–4499 (2000) .

[6] J. A. Sanders and F. Verhulst, *Averaging Methods in Nonlinear Dynamical Systems* (Springer, New York, 1985).

[7] S. Wiggins, *Introduction to Applied Nonlinear Dynamical Systems and Chaos* (Springer, New York, 1990).

[8] A. J. Lichtenberg and M. A. Lieberman, *Regular and Stochastic Motion* (Springer, New York, 1983).

[9] R. C. Hilborn, *Chaos and Nonlinear Dynamics* (Oxford University Press, New York, 1994).

[10] J. Guckenheimer and P. Holmes, *Nonlinear Oscillations, Dynamical Systems, and Bifurcations of Vector Fields* (Springer, New York, 1983).

[11] A. V. Buryak, I. Towers, and S. Trillo, Phys. Lett. A **267**, 319–325 (2000).

[12] H. E. Nusse and J. A. Yorke, *Dynamics: Numerical Explorations* (Springer, New York, 1991).